JOURNAL OF SOLID STATE CHEMISTRY, 10, 72–94 (1974)

An Electron Microscope Study of the FeO–Fe_2O_3–TiO_2 System and of the Nature of Iron-Doped Rutile

L. A. BURSILL*

School of Chemistry, University of Western Australia, Nedlands, 6009, Australia

Received May 7, 1973

An electron microscope study of FeO–Fe_2O_3–TiO_2 reveals a wide range of unsuspected *CS* behavior. At 1300°C, isolated {132} faults ($MX_{1.995}$) coexist with aggregated {121} *CS* planes ($MX_{1.97}$). At lower temperatures, no aggregated faults occur and isolated faults swing towards {011}; these are often stepped and are accompanied by a high dislocation density. Above 1400°C, elements of (121) and (132) intergrow, forming intermediate high-index *CS* structures whose indices depend on oxygen/metal ratio, Fe^{3+}/Fe^{2+} ratio, and temperature. At a given temperature, and in air, there is a range of oxygen/metal ratios where the *CS* plane swings continuously from (132) to (121); the width of this range increases with increasing temperature (1.97–1.93 at 1500°C). The observations suggest a mechanism for transforming from rutile to α-PbO_2-derived *CS* structures. Pseudobrookite is incoherent with rutile, coexisting with slightly reduced rutile ($MX_{1.995}$) below about 1200°C but with ordered *CS* structures above this. Wavy domain boundaries and a new superstructure appear in beam-heated pseudobrookite.

I. Introduction

Numerous ordered structures M_nO_{2n-p} ($4 \leqslant n \leqslant \infty$, $1 \leqslant p \leqslant \infty$) have been found in reduced titanium and titanium + chromium oxides. A review of the structural principles, texture, reaction mechanisms, and thermodynamics showed quantitative differences between these two systems (*1*). It therefore seemed worthwhile to study the behavior of other trivalent cations in rutile. X-ray phase analysis (*2*, *3*) showed that approx 3 mole% Fe_2O_3 may be dissolved in TiO_2 before pseudobrookite (Fe_2TiO_5) appeared. No homologous series were reported or suspected. We found that 2.5 mole% Fe_2O_3 produced {132}[1] faults of the same type as occurred in $TiO_{1.995}$ (*1*) (unpublished results, 1970). Recently, other workers claimed (*4*) that {120} faults occurred in iron-doped rutile. We thought that these conflicting results may indicate reduction of Fe^{3+} to Fe^{2+} in one case and therefore undertook a systematic electron microscopy/diffraction study of TiO_2 + 0–25 mole% Fe_2O_3. A wide range of heat-treatment times and conditions were used in an attempt to understand the reaction mechanisms involved in the production, ordering, and cooperative reorientation of the *CS* planes.

II. Previous Phase Analyses

Known phase relations for the system iron oxide–titanium oxide, in air at temperatures close to the liquidus, are shown in Fig. 1a (*2*). Isothermal sections through the system FeO–Fe_2O_3–TiO_2 at 1200°C (*3*) and 1300°C (*5*) are given in Fig. 1b, c. Note the oxygen isobar corresponding to preparations heated in air, and the occurrence of the ternary solid solutions magnetite–ulvospinel (Fe_3O_4–Fe_2TiO_4), hematite–ilmenite (Fe_2O_3–$FeTiO_3$) and ferric/ferrous pseudobrookite (Fe_2TiO_5–$FeTi_2O_5$). Thus heating mixtures of Fe_2O_3

* Present address: School of Physics, University of Melbourne, Parkville, 3052, Australia.

[1] Indices without subscript refer to rutile cell or subcell.

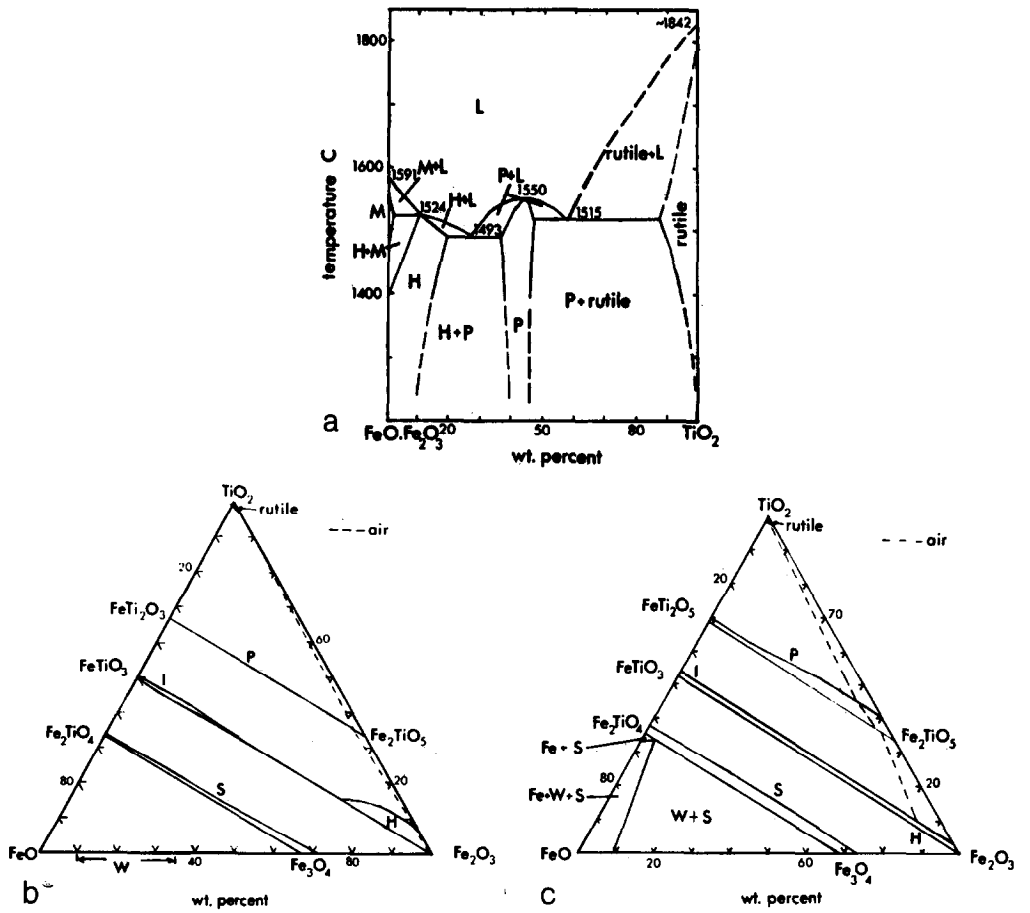

FIG. 1. (a) Phase relations in the system iron oxide–titanium oxide in air, after MacChesney and Muan (*2*). The system is not binary. Abbreviations are W = wüstite, M = magnetite, H = hematite, U = ulvöspinel, I = ilmenite, P = pseudobrookite, and L = liquid.

(b) The 1200°C isothermal section through FeO–Fe_2O_3–TiO_2, after Webster and Bright (*3*).

(c) The 1300°C isothermal section through the system FeO–Fe_2O_3–TiO_2, after Taylor (*5*). Heavy lines are boundary curves and light dash curves are the oxygen isobars for air.

and TiO_2 in air above 1300°C produces phases in the ternary system FeO–Fe_2O_3–TiO_2 and not those of the pseudobinary Fe_2O_3–TiO_2. Consideration of the free energies of formation of the various lower oxides of iron and titanium shows (*2*) that there is danger of reducing Ti^{4+} to Ti^{3+} only if all the iron is reduced to the ferrous state. (Such strongly reducing conditions were not used in this study.)

The stability ranges reported for the rutile and pseudobrookite phases are as follows. At 1200°C, in air, the pseudobrookite phase first appeared at about 3 mole% Fe_2O_3, i.e., $MX_{1.97}$ (*3*). No composition range was reported for pseudobrookite. At 1300°C, in air, the limit of the rutile phase (read off Fig. 3 in Ref. (*5*)) apparently occurs at 96 wt% TiO_2 + 2.5 wt% Fe_2O_3 + 1.5 wt% FeO, i.e., $MX_{1.971}$ with $Fe^{3+}/Fe^{2+} = 1.5$. Pseudobrookite was reported to have a composition range from 45 wt% TiO_2 + 52 wt% Fe_2O_3 + 3 wt% FeO to 34 wt% TiO_2 + 64.4 wt% Fe_2O_3 + 1.5 wt% FeO, i.e., from $MX_{1.707}$ to $MX_{1.661}$ with Fe^{3+}/Fe^{2+} from 15.5 to 38.7. At 1500°C, in air, the rutile "solid solution" limit was apparently 85 wt% TiO_2 +

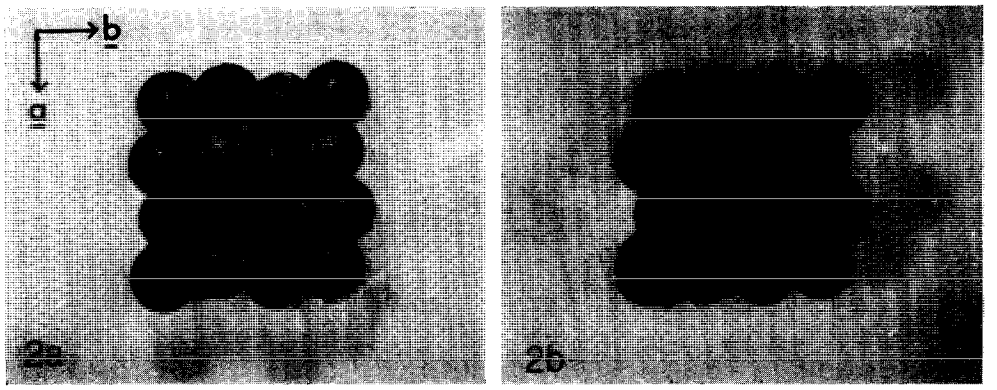

FIG. 2. (a) [001] projection of rutile, large and small balls represent oxygen and titanium, respectively. Both (100) and (010) oxygen planes are puckered. Note the *c*-axis channels.

(b) Idealized rutile structure with h.c.p. anions. (100) planes are flat. Note the exaggerated puckering of (010) planes and the closed-up channels.

10 wt% Fe_2O_3 + 5 wt% FeO, i.e., $MX_{1.894}$ ($Fe^{3+}/Fe^{2+} = 1.8$) (read off Fig. 2 in Ref. (*2*)). The pseudobrookite composition range is estimated to be approx $MX_{1.66}$ to $MX_{1.72}$.

One more phase, $Fe_2Ti_3O_9$, has been reported (*6*). It was stable only below 800°C and may be derived from α–PbO_2 type structure by *CS* (*7*).

III. Structural Background

The [100] projection of rutile suggests that the oxygens are in approx h.c.p., but projection along [001] shows that (100) planes are puckered (Fig. 2a). Titanium lies in rows of edge-shared octahedral interstices parallel to *c*. Adjacent rows are joined by corner-sharing. We may idealize the structure to perfect h.c.p. by rotating [001] edge-shared rows in a cog-wheel action until (100) planes are flat (Fig. 2b, $\frac{1}{2}[0\bar{1}1]$ is then precisely an oxygen–oxygen vector. Such idealization exaggerates puckering on (010) and closes the *c*-axis channels which in real rutile form a continuous column of octahedrally coordinated sites at $\frac{1}{2}00$, $\frac{1}{2}0\frac{1}{2}$, $\frac{1}{2}01$, etc. $\frac{1}{2}0\frac{1}{2}$ is retained but $\frac{1}{2}00$ is split into two tetrahedral interstices. Rutile has a two-layer repeat ...*ababab*... parallel to (100). Fig. 3a shows the pattern of filled sites on an *a* layer, this same pattern is repeated between *b* and *a* but with the filled sites in one layer immediately above and below empty octahedral interstices in adjacent layers.

Rutile has been transformed to the α–PbO_2 type structure in high-pressure experiments (*8*) when it becomes orthorhombic ($a_\alpha = 4.529$ Å, $b_\alpha = 5.464$ Å, $c_\alpha = 4.905$ Å). It may also be idealized to h.c.p. anion layers parallel to $(100)_\alpha$ when Ti occupies half the octahedral holes forming zig-zag chains of edge-shared octahedra mutually connected by corner-sharing (Fig. 3b). If adjacent (011) oxygen planes are sheared by $\frac{1}{2}[0\bar{1}1]$, we obtain the stoichiometric antiphase boundary $\frac{1}{2}[0\bar{1}1](011)$. The *c*-axis strings of rutile are now stepped but each TiO_6 octahedron still shares two edges and six vertices (Fig. 3c). Repetition of this operation on every second (011) oxygen plane produces α–PbO_2, whereas on every plane it produces a rutile twin (Fig. 3d).

Extra cations may be accommodated into rutile with minimum face-sharing if they add in $[1\bar{1}1]$ chains at the antiphase boundary (*1*). This generates a corundum-like chain of octahedra-sharing faces parallel to [100] and edges parallel to $[0\bar{1}1]$. Both α-Fe_2O_3 (hematite) and $FeTiO_3$ (ilmenite) have the corundum structure. As the proportion of corundum-type steps (*C*) to α–PbO_2 type steps (*A*) increases (Fig. 4), the antiphase boundary becomes increasingly nonstoichiometric and climbs away from (011), eventually to (121),

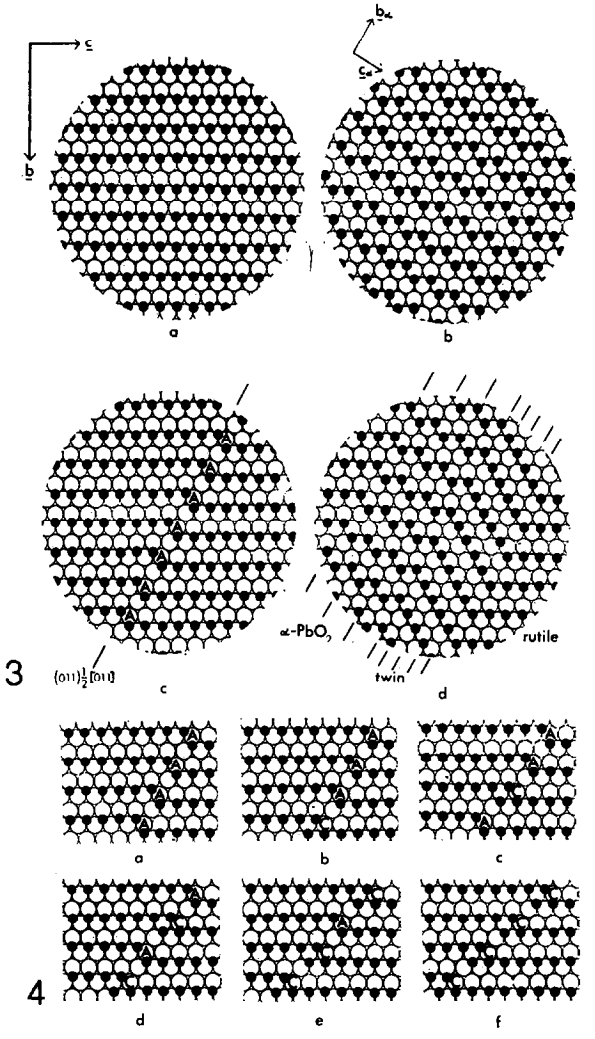

FIG. 3. (a) Filled octahedral interstices on (100) layer of rutile.
(b) Filled octahedral interstices on $(100)_\alpha$ layer of α–PbO_2.
(c) Stoichiometric antiphase boundary (*APB*) $(011)\frac{1}{2}[0\bar{1}1]$ in rutile. Note the *APB* steps *A*.
(d) Lamellae of α–PbO_2 and rutile microtwin produced by repeating the *APB* operation on every second or on every (011) oxygen plane.

FIG. 4. (100) layer of rutile with (a) an *APB* proceeding, by the introduction of extra cations at corundum type steps *C* and the jumps shown in (b) and (c), to a segment of (132) *CS* plane in (d) and to a (121) *CS* plane in (e) and (f).

when all the *A* steps have been eliminated. The displacement across the *CS* plane is always $\frac{1}{2}[0\bar{1}1]$. In principle, *any* of the high-index boundaries $(hkl) = p.(121) + q.(011)$ can be generated by controlling the sequence of *C* and *A* steps. *p* and *q* are the number of *C* and *A* steps per repeat distance along the *CS* plane. We may therefore, at least in principle, generate a continuous series of ordered structures by varying the proportions *p* and *q* along the boundary and/or the proportions *P* and *Q* of different spacings normal to the *CS* plane. Both ordered and disordered intergrowth structures occur in $(Ti^{4+}, Ti^{3+})O_x$

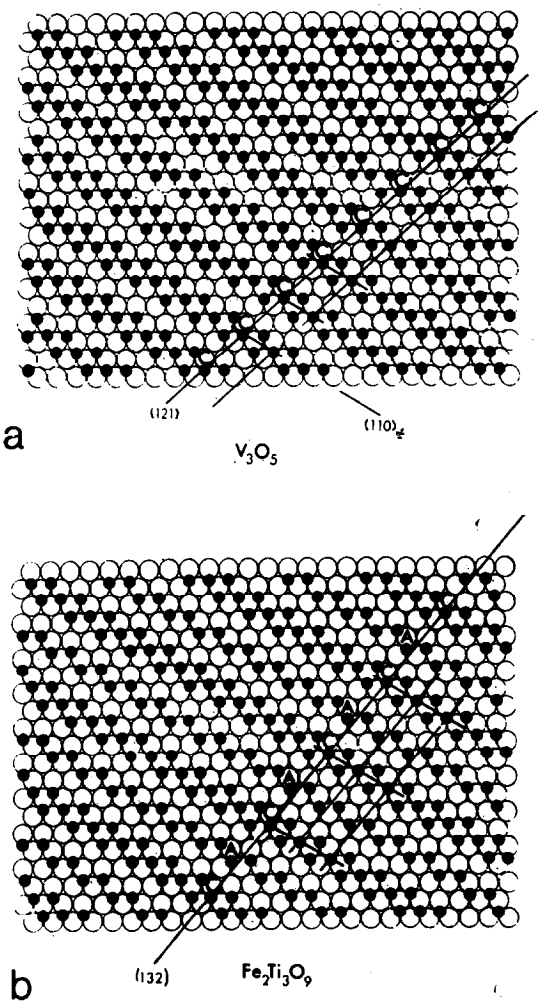

FIG. 5. (a) (100) layer of V_3O_5 showing (121) and $(110)_\alpha$ *CS* planes.

(b) An intergrowth structure $M_5O_9 = M_3O_5 + M_2O_4$ ($P = 1$, $Q = 1$), consisting of alternate slabs of V_3O_5 and α–PbO_2 intergrown on $(110)_\alpha$ planes. Alternatively, it is one of a family M_nO_{2n-1} with $n = 5$ derived from rutile by the operation $(132)\frac{1}{2}[0\bar{1}1]$. A unit cell of $Fe_2Ti_3O_9$ is outlined.

and $(Ti^{4+}, Cr^{3+})O_x$ (*1*). Methods for determining the *CS* plane indices (*hkl*) and the oxygen/metal ratio x from the diffraction patterns (*1*) rely on the fact that all planes $(hkl) = p.(121) + q.(011)$ lie in the $[1\bar{1}1]$ zone, which must be obtained by painstaking tilting experiments.

The series of structures M_nO_{2n-P} ($n = 3P + 2Q$) derived from α–PbO_2 by the *CS* operation $(110)\frac{1}{2}[010]_\alpha$ may be described (*7*) as intergrowths $P.M_3O_5 + QM_2O_4$, where M_3O_5 has the V_3O_5 structure and M_2O_4 is α–PbO_2 (Fig. 5a). In view of the above simple relation between rutile and α–PbO_2, it is not suprising that these are in fact special cases of the series proposed for *CS* in rutile (*9*). Thus $n = 5(110)_\alpha$ is identical to $n = 5(132)$ (Fig. 5b). This is $Fe_2Ti_3O_9$ (cell parameters $a = 7.071$ Å, $b = 4.997$ Å, $c = 18.862$ Å, $\alpha = 90°$, $\beta = 119.56°$, $\gamma = 90°$). It was reported to decompose above 800°C, giving pseudobrookite plus rutile (*6*). A matrix relating $(110)\frac{1}{2}[010]_\alpha$ *CS* structures to the α–PbO_2 subcell is

	α–PbO_2		
	1	−1	0
M_nO_{2n-P}	0	0	1
$(n = 3P + 2Q)$	0	$-(5P/4 + Q)$	$P/2$.

Pseudobrookite is orthorhombic with $a_{pb} = 9.79$ Å, $b_{pb} = 9.93$ Å, $c_{pb} = 3.72$ Å. The continuous solid-solution Fe_2TiO_5–$FeTi_2O_5$ has been reported (*6*) but precise atomic coordinates have not been determined for ferrous pseudobrookite.

IV. Experimental

Preparations of $Ti_{n-2}Fe_2O_{2n-1}$ with $n = 5$, 10, 20, and 40 were given various heat treatments (Table I). The starting powders, TiO_2 and Fe_2O_3 (Koch–Light 3N), were mixed, pressed into 1-g pellets, and given preliminary reactions in air at 900°C for 1 week in an open platinum boat. These fine-grained sintered pellets were given further reactions in small platinum tubes. The products were identical whether the tubes were open or sealed. They were cooled to room temperature by quickly pulling from the furnace. Oxygen/metal and Fe^{3+}/Fe^{2+} ratios were calculated for our preparations using the detailed results of Refs. (*2*, *3*, *5*).

Preparations 1.7 and 1.8 were designed to maintain iron as Fe^{2+}. 1.7 was mixed as before but heated in an evacuated quartz tube containing, but not in contact with, a pellet of net stoichiometry $Fe_{1.02}O$ made by hydrogen reduction of Fe_2O_3. It maintained the oxygen partial pressure to a value defined by the iron/

TABLE I

PHASE ANALYSIS OF THE SYSTEM $FeO–Fe_2O_3–TiO_2$ IN AIR[a]

Sample	Oxygen/metal Ratio: Prepared value[b]	Oxygen/metal Ratio: Estimated value[c]	Heat Treatment	Structures found by electron microscopy
1.1	1.975	1.970[g] (2.5)	1300°C, 2 days, sealed tube	MX_2{011} $MX_{1.998}${132} $MX_{1.97}${121} $MX_{1.98-1.988}${121 + 132}
1.2	1.975	1.970[g] (2.5)	1300°C, 7 days, sealed tube	MX_2 $MX_{1.99}${132} $MX_{1.97}${121} Pb
1.3	1.975	1.970[g] (2.5)	1300°C, 16 days, sealed tube	MX_2 $MX_{1.993}${132} $MX_{1.97}${121}
1.4	1.975	1.968[e] (1.0)	1400°C, 14 days, open tube	$MX_{1.995}${132} $MX_{1.963}${121}
1.5	1.975	1.965[e] (1.0)	1500°C, 3 days, open tube	$MX_{1.947-1.955}${495–121}
1.6	1.975	1.975[h]	1500°C, 7 days, then 1200°C, 19 days, sealed tube	MX_2 $MX_{1.999}${132} Pb
1.7	1.975	1.95[f] (black color)	1140°C, 1 day, sealed quartz tube with Fe/FeO buffer	MX_2{011 + dislocations}
1.8	1.975	1.975[f]	1300°C, dynamic vacuum 2×10^{-6} torr, 16 days	MX_2{011 + steps}. Also microtwins and dislocations
2.1	1.95	1.937[g] (5.0)	1300°C, 7 days, sealed tube	MX_2{011} $MX_{1.999}${132} $MX_{1.97}${121} Pb
2.2	1.95	1.930[e] (1.0)	1450°C, 4 days, sealed tube	$MX_{1.994}${121} $MX_{1.952-1.960}${5, 11, 6–253}
2.3	1.95	1.930[e] (1.0)	1500°C, 3 days, sealed tube	$MX_{1.937-1.944}${121}
2.4	1.95	1.930[e] (1.0)	1500°C, 7 days, open tube	$MX_{1.94}${121}
2.5	1.95	1.930[e] (1.0)	1480°C, 7 days, open tube	$MX_{1.95}${5, 11, 6–121}
2.6	1.95	1.937[e] (1.0)	1450°C, 4 days, then 1300°C, 7 days, sealed tube	$MX_{1.995}${132} $MX_{1.97}${121} $MX_{1.991}${143} Pb
2.7	1.95	1.95[h]	1500°C, 7 days, then 1200°C, 20 days, open tube	$MX_{1.999}${132} $MX_{2.0}${close to 011} Pb
2.8	1.95	1.95[h]	1500°C, 7 days, then 1100°C, 28 days, open tube	$MX_{1.0}${011 + stepped 011} Dislocations. Pb
3.1	1.90	1.887[g] (6.5)	1300°C, 14 days, sealed tube	$MX_{1.999}${132} $MX_{1.97}${121} Pb

TABLE I—*continued*

Sample	Oxygen/metal Ratio: Prepared value[b]	Oxygen/metal Ratio: Estimated value[c]	Heat Treatment	Structures found by electron microscopy
3.2	1.90	1.86[e] (1.0)	1450°C, 7 days, sealed tube	$MX_{1.935-1.946}${253–121} $MX_{1.94}${disordered high index} Pb
3.3	1.90	1.86[e]	1500°C, 7 days, sealed tube	$MX_{1.935-1.940}${495} Pb
3.4	1.90	1.90[h]	1500°C, 7 days, then 20 days at 1200°C, open tube	MX_2{dislocations} $MX_{1.999}${132} Pb
4.1	1.80	1.781[g] (9.9)	1300°C, 14 days, sealed tube	$MX_{2.0}${011} $MX_{1.999}${132} Pb
4.2	1.80	1.715[d] (1.3)	1450°C, 7 days, sealed tube	Pb
4.3	1.80	1.715[d] (1.3)	1500°C, 7 days, open tube	Pb
4.4	1.80	1.80[h]	1500°C, 7 days then 1100°C, 28 days, open tube	Pb $MX_{2.0}${stepped 011}

[a] Values in parentheses are Fe^{3+}/Fe^{2+} ratios. $MX_x\{hkl\}$ indicates stoichiometry and *CS* plane indices of rutile-derived structures. Pb indicates pseudobrookite.
[b] Assuming Fe^{3+} only.
[c] Using footnotes *d–h*.
[d] Measured in Ref. (*6*).
[e] Estimated from Ref. (*6*).
[f] Assuming Fe^{2+} only.
[g] Measured in Ref. (*12*).
[h] Estimated from Ref. (*7*).

wüstite equilibrium. Black, rather than brown pellets resulted. 1.8 was made by mixing $Fe_{1.02}O$ and TiO_2 powders and annealing in an oxygen-free atmosphere. Black products ensued.

Specimens were prepared for electron microscopy as described previously (*9*) and examined with an Elmiskop 101 with goniometer cartridge until no new features appeared on at least two successive microscope sessions.

V. Observations

Examination of the 900°C preparations was unsuccessful as the small grains did not fracture but were too thick to transmit electrons. All other preparations yielded large grains (approx 10^{-2} mm diam) which fractured to give suitable thin edges.

1. $(Ti, Fe)O_{1.975}$

1.1 [1300°C, 2 days, sealed tube]. The predominant contrast was a maze of planar faults (Fig. 6a). Tilting faults edge-on (Fig. 6b) showed them to be mostly on {132} with a small proportion on {011}. Any of the eight {132} or four {011} faults may appear in a maze. They were not always perfectly straight or exactly parallel to low-index planes (Fig. 6b). To distinguish the faults (*hkl*), it is essential to obtain $[1\bar{1}1]$ zones (Fig. 6c). Diffraction

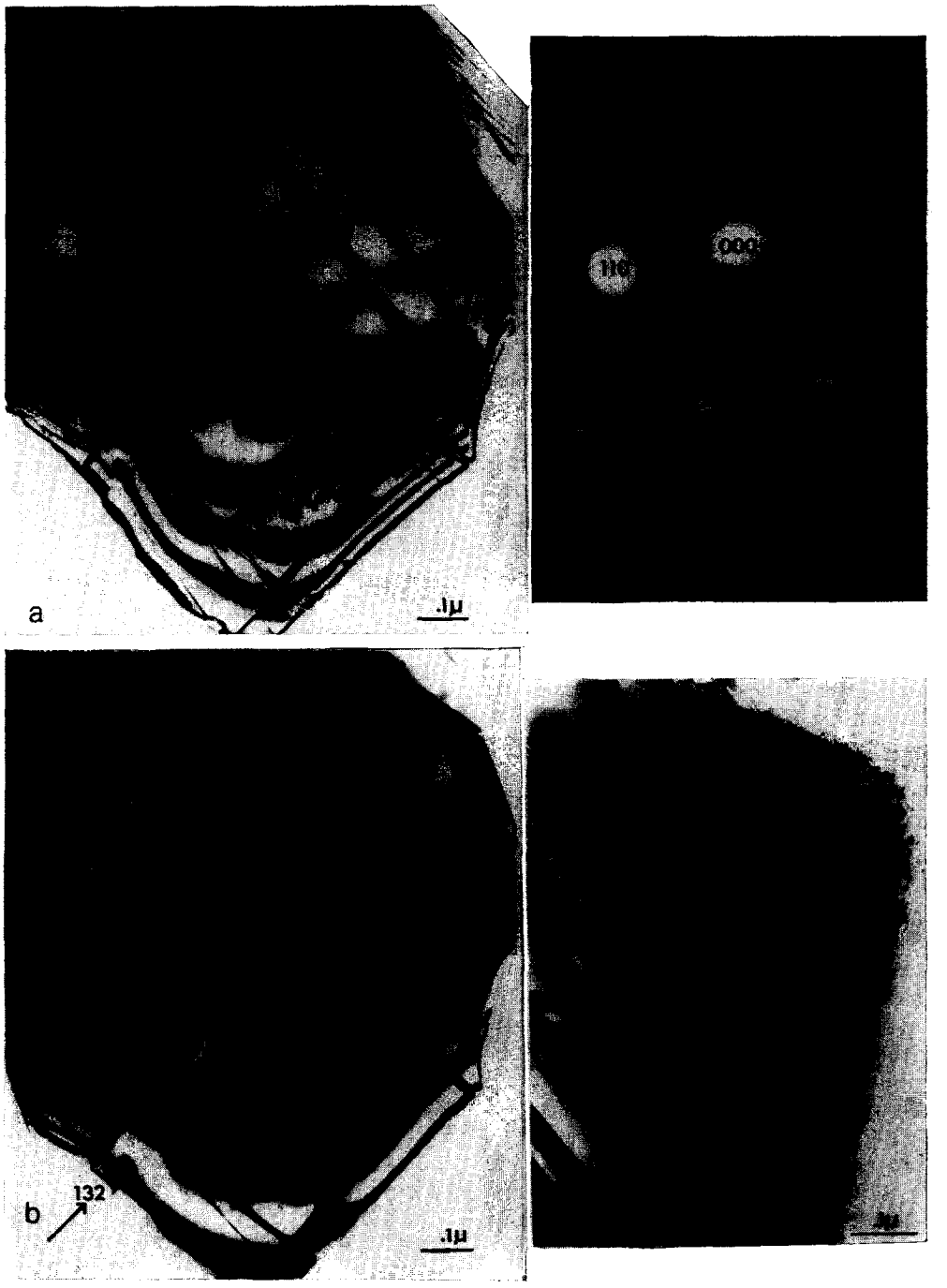

FIG. 6. (a) $(Ti,Fe)O_{1.975}$ (1.1). Maze of planar faults in a rutile matrix.

(b) Area of 6(a) tilted into the $[1\bar{1}1]$ zone. (132) and $(13\bar{2})$ are edge-on. Note small orientation changes for some faults.

(c) $[1\bar{1}1]$ diffraction pattern of 6(b).

(d) Area to the left of 6(a) showing zig-zag {121} faults.

contrast experiments showed the effective fault vectors were as for TiO_x, i.e., approx $\frac{1}{2}[0, -0.90, 0.90](132)$ and $\frac{1}{2}[0\bar{1}1](011)$, cf. Ref. (*10*). As shown in Ref. (*1*), ordered (*hkl*) faults give a family M_nO_{2n-p} with spacings $D_{hkl} = d_{hkl}(n - p/2)$, where d_{hkl} is the spacing of (*hkl*) planes. Thus the mean spacing of 600 Å for (132) faults in Fig. 6b corresponds to $MX_{1.998}$.

The next most common feature was bands of closely spaced zig-zag faults (Fig. 6d) which indexed as {121} when oriented edge-on in the $[1\bar{1}1]$ zone. These could conceivably be mistaken for {120} for some orientations. The (121) fault spacing (50 Å) corresponds to $MX_{1.97}$. The characteristic texture is slabs of slightly reduced rutile ($MX_{1.998}$), consisting of a maze of {132} and {011} faults, criss-crossed by bands of zig-zag {121} faults ($MX_{1.97}$). However, in one crystal the fault spacings and orientations were very complex (Fig. 7a). Tilting into the $[1\bar{1}1]$ zone (Fig. 7b) revealed a subtle, ill-defined domain texture, groups of aligned (132) and (121) faults occur but the orientation varies along their length. The mean spacing (approx 80 Å) corresponds to $MX_{1.98}$ for (121) and to $MX_{1.988}$ for (132). The faults are remarkably continuous despite changes in orientation. The diffraction pattern showed streaking along both 132 and 121 reciprocal lattice vectors. Additional spots are intersections of the Ewald sphere with streaks along other {132} reciprocal lattice vectors (*11*).

A few crystals showed complex strain contrast (Fig. 8) which may be precipitates of pseudobrookite although no diffraction spots confirmed this. Despite repeated attempts, orienting many faults edge-on, no {120} faults were found, either in this specimen or in any of the following iron-doped rutiles. A preparation of gallia-doped rutile did show {120} faults!

1.2 [*1300°C, 7 days, sealed tube*]. Many areas like Fig. 6 were found but there were no complex mixtures like Fig. 7 or strain contrast as in Fig. 8. A new feature was a small number of large flakes of pseudobrookite. These were readily identified by the 9.93 Å $(010)_{pb}$ and 9.79 Å $(100)_{pb}$ reflections and by the perfection of the lattice images which showed a very low density of dislocations (Fig. 9a, b). No rutile/pseudobrookite interfaces were found. These exist as separate grains, sometimes visible in the optical microscope.

1.3 [*1300°C, 16 days, sealed tube*]. The faults were now definitely segregated into areas containing {132} and areas of zig-zag {121} faults. Note the relatively high degree of alignment of (132) faults in Fig. 10a, where the mean spacing 150 Å corresponds to $MX_{1.993}$. Although the diffraction pattern (Fig. 11b) suggests the {121} faults order, the corresponding micrographs (Fig. 11a) shows only islands of order consisting of some 3–10 faults regularly spaced and aligned over only part of their length, giving a wide range of lamellae widths, lengths, spacings, and (twin) orientations. The mean spacing of approx 60 Å corresponds to $MX_{1.97}$. No pseudobrookite was found.

1.4 [*1400°C, 14 days, open tube*]. Isolated {132} and aggregated zig-zag faults again occurred with a preponderance of the latter. The spacing was approx 45 Å, i.e., $MX_{1.963}$.

1.5 [*1500°C, 3 days, open tube*]. Diffraction patterns from practically every flake showed rows of very sharp superlattice spots along $(hkl) = p.(121) + q\cdot(011)$ with $p/q \geqslant 4$ but mostly very close to (121) (Fig. 12a–c). The spacing corresponds to 32–37 Å, i.e., $MX_{1.947-1.955}$. Only a small proportion of flakes showed widely spaced {132} faults. High-resolution images of (495) faults (Fig. 13a) showed them to be very straight and regularly spaced. Zig-zag lamellae were much wider. Fig. 13b shows dagger-shaped twins inside a slab of (121) faults. They appear to be annealing out. This same mechanism could operate for insertion. A new feature of 1500°C samples was some instability in the beam. This was avoided by selecting thin crystals and using lower beam intensities. No pseudobrookite was found.

1.6 [*1500°C, 7 days, then 1200°C, 19 days, sealed tube*]. The predominant feature was large flakes containing a very low density of {132} faults (Fig. 14) corresponding to $MX_{1.999}$. Pseudobrookite occurred. A small proportion of areas showed zig-zag {121} faults. Strain contrast also occurred (cf. Fig. 8).

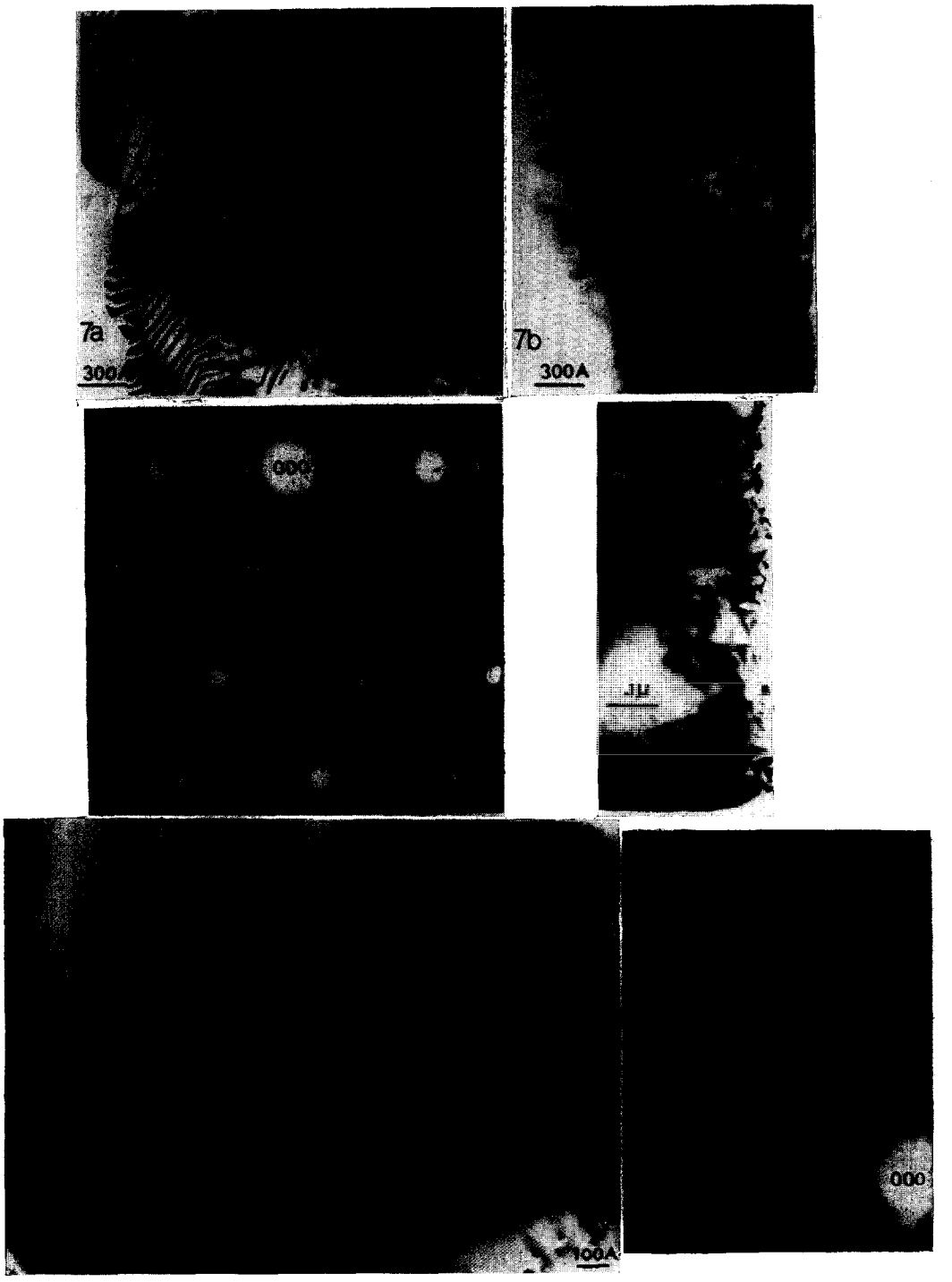

FIG. 7. (a) $(Ti,Fe)O_{1.975}(1.1)$. Chaotic fault texture in iron-doped rutile.

(b) Area of 7(a) after tilting into $[1\bar{1}1]$ zone. Faults oscillate between (132) and (121) producing ill-defined domain texture. Unidentified inclined faults occur in alternate lamellae.

FIG. 8. $(Ti,Fe)O_{1.975}(1.1)$. Precipitate strain contrast in rutile.

FIG. 9. (a) $(Ti,Fe)O_{1.975}(1.2)$. Lattice image of pseudobrookite showing 9.79 Å $(100)_{pb}$ fringes.

(b) Diffraction pattern of 9(a) showing $[01\bar{1}]_{pb}$ zone.

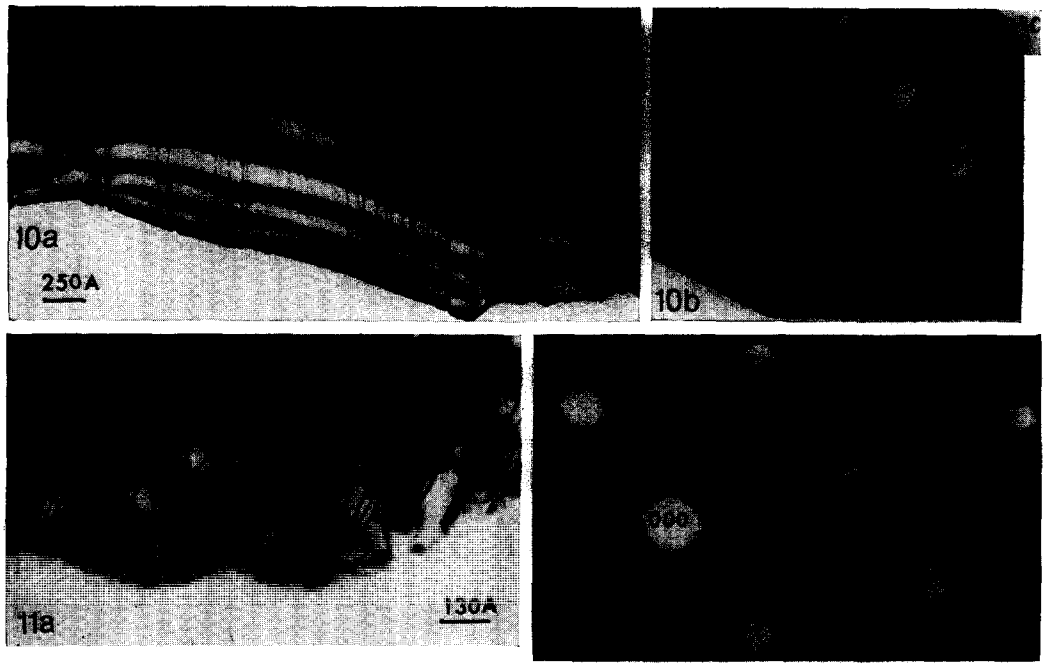

FIG. 10. (a) $(Ti,Fe)O_{1.975}$(1.3). Aligned (132) faults with mean spacing approx 150 Å, i.e., $MX_{1.993}$.
(b) [1$\bar{1}$1] diffraction pattern of 10(a) showing streaking parallel to g(132).

FIG. 11. (a) $(Ti,Fe)O_{1.975}$(1.3). Mainly {121} faults ($MX_{1.97}$) with islands of order consisting of a small number of faults regularly spaced and aligned over only part of their length.
(b) [1$\bar{1}$1] zone of 11(a) showing the apparent development of a 60 Å period.

1.7 [1140°C, 1 day, sealed quartz tube with "FeO" buffer]. Rutile flakes contained an unusually high density of dislocations, occurring singly, in small groups, or in extensive walls. These were accompanied by {011} faults (Fig. 15a). Some areas contained closely spaced {011} faults (Fig. 15b) which were often stepped with dotted strain contrast along their length. Figure 15d, e shows fine structure in some faults. The diffraction patterns showed, in the [1$\bar{1}$1] zone, streaking parallel to g(011) plus sharper streaks parallel to high-index reciprocal lattice vectors inclined at about 2–5° to g(011), in a direction towards (132). No {132} or {121} faults and no pseudobrookite could be found.

1.8 [$(Fe^{2+}, Ti)O_{1.975}$, open Pt tube inside a mullite outer tube at 1300°C for 16 days with dynamic vacuum 2×10^{-6} torr]. No {hkl} faults were found. Most flakes showed fine-scale microtwinning (Fig. 16a) with streaking parallel to g(011). Spots developed in rutile twin positions (Fig. 16b, c) with variable sharpness. (011) faults were mostly irregularly spaced (Fig. 16d) and sometimes stepped (cf. Fig. 15). A wide range of dislocations, from isolated to tangles and complex low angle boundaries, was observed.

2. $(Ti, Fe)O_{1.95}$

2.1 [1300°C, 7 days, sealed tube]. A maze of {132} faults in rutile predominated (cf. Fig. 6a) with mean spacing corresponding to $MX_{1.999}$. Bands of {121} faults occurred in similar proportions as found in 1.1. Some {011} faults also occurred and well-ordered flakes of pseudobrookite appeared with greater frequency than for 1.2.

2.2 [1450°C, 4 days, sealed tube]. Wide lamellae of high-index *CS* structures predominated in two-thirds of the flakes (Fig. 17a). The *CS* plane was mostly between (253) and (5, 11, 6), the spacing was 31 ± 2 Å, corresponding to stoichiometries from $MX_{1.960}$ for

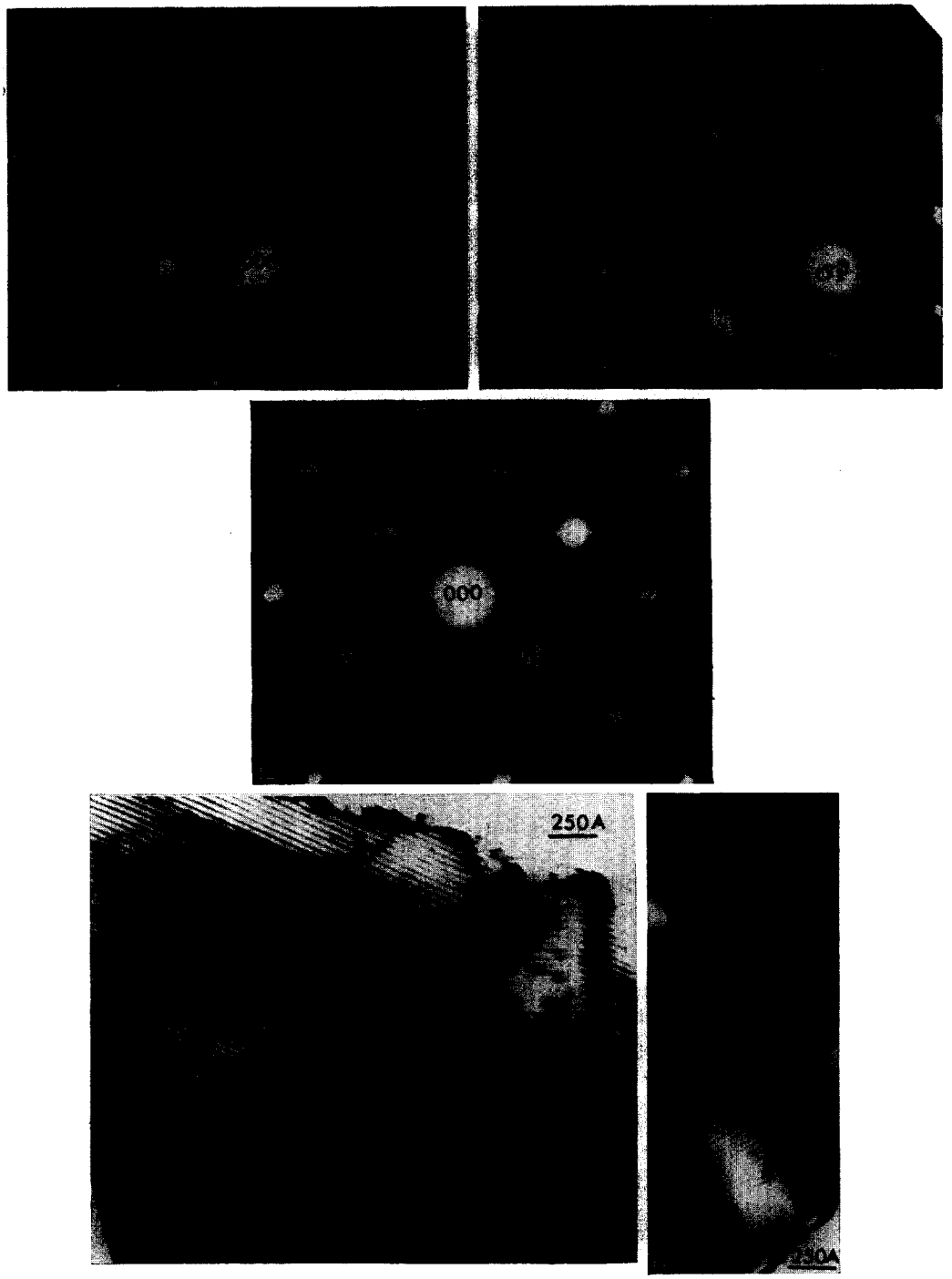

FIG. 12. $(Ti,Fe)O_{1.975}(1.5)$. $[1\bar{1}1]$ zones showing superlattice rows along 495, almost 121, and exactly 121.

FIG. 13. (a) $(Ti,Fe)O_{1.975}(1.5)$. High-resolution image of ordered (495) faults (area of 12(a)). The diffuse black contrast does not occur on every lattice image and is of unknown origin.

(b) Dagger-shaped twins apparently in the process of annealing out.

FIG. 14. $(Ti,Fe)O_{1.975}$(1.6). Low density of (132) faults in rutile.

(253) to $MX_{1.952}$ for (5, 11, 6). The remaining flakes showed disordered *CS* planes. For example, Fig. 17b shows that both the spacing (approx 30 Å) and the orientation (approx (253)) vary. In some areas, widely spaced {121} faults (100–600 Å, i.e., $MX_{1.990-1.998}$) coexisted with rutile. No pseudobrookite was found.

2.3 [1500°C, 3 days, sealed tube]. Zig-zag twins of regularly spaced {121} faults predominated (Fig. 17c) with spacings (25–31 Å) corresponding to $MX_{1.937-1.944}$. No {132} faults and no pseudobrookite occurred.

2.4 [1500°C, 7 days, open tube]. Two types of structure appeared. Predominant was finely twinned rutile with diffuse $[1\bar{1}1]$ diffraction patterns (Fig. 18), characteristic of melted rutiles. The second was an ordered superstructure not found previously (Fig. 19a). Attempts to index Fig. 19a using α–PbO_2-derived indices proved incorrect. In fact, the superlattice rows were normal to (100) of rutile. The superlattice period was 28.5 Å. Figure 19b shows the corresponding lattice image. A detailed study of this structure is in progress. It appears to be related to the regular twinning often observed at high temperatures (cf. Fig. 17a) where the twin composition plane is often (100).

2.5 [1480°C, 7 days, open tube]. Rutile-derived *CS* structures identical to 2.2 and 2.4 occurred.

2.6 [1450°C, 4 days, then 1300°C, 7 days, sealed tube]. Bands of widely spaced {132} faults alternated with bands of aggregated faults (Fig. 20a). The diffraction patterns showed streaking parallel to (132) and (121) (Fig. 20b). {011} faults occurred in some areas and some (143) *CS* planes appeared (note that (143) = (132) + (011)). Pseudobrookite appeared.

2.7 [1500°C, 7 days, then 1200°C, 20 days, open tube]. A low density of {132} faults predominated (cf. Fig. 14) with $MX_{1.999}$. {011} faults also occurred and large perfect flakes of pseudobrookite were common. No {121} faults appeared.

2.8 [1500°C, 7 days, then 1100°C, 28 days, open tube]. Most crystals exhibited a low density of faults accompanied by an unusually high density of dislocations (cf. 1.6, 1.7) and dislocation tangles (cf. Fig. 20b). When oriented edge-on, the faults indexed as {011} and some high-index faults within about 2° of {011}. Many large perfect flakes of pseudobrookite were found.

3. $(Ti, Fe)O_{1.90}$

3.1 [1300°C, 14 days, sealed tube]. Large areas of aligned (132) and zig-zag {121} faults

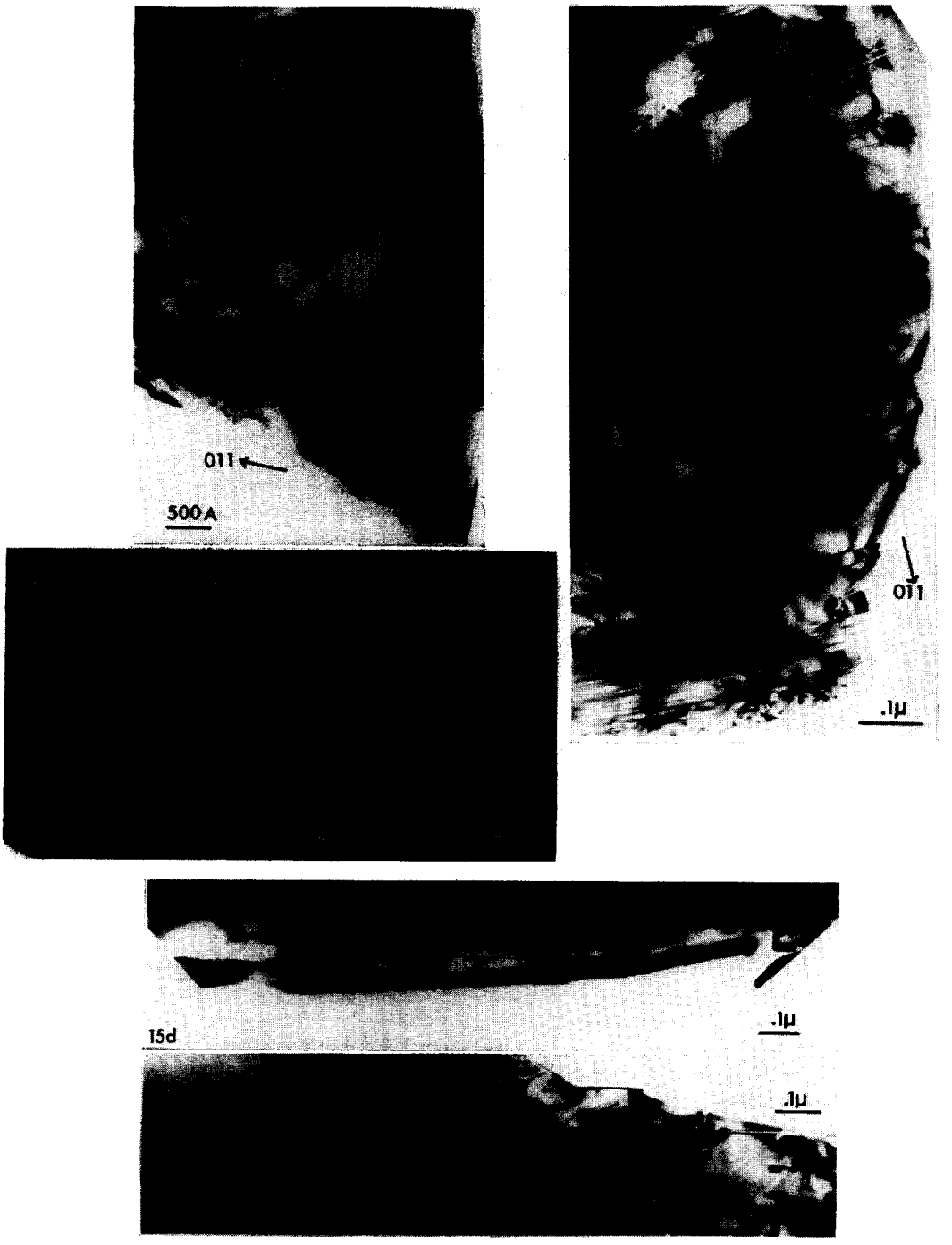

FIG. 15 (a) $(Ti,Fe)O_{1.975}$(1.7). Dislocations and (011) faults in rutile.

(b) High density of "011)" faults, rows of dotted contrast occur at steps on the faults. Many dislocation tangles will be seen.

(c) [1$\bar{1}$1] zone of 15(b) showing streaking along 011 plus sharper streaks inclined at approx 3° to 011 in a direction towards 132.

(d, e) Fine structure of stepped (011) faults.

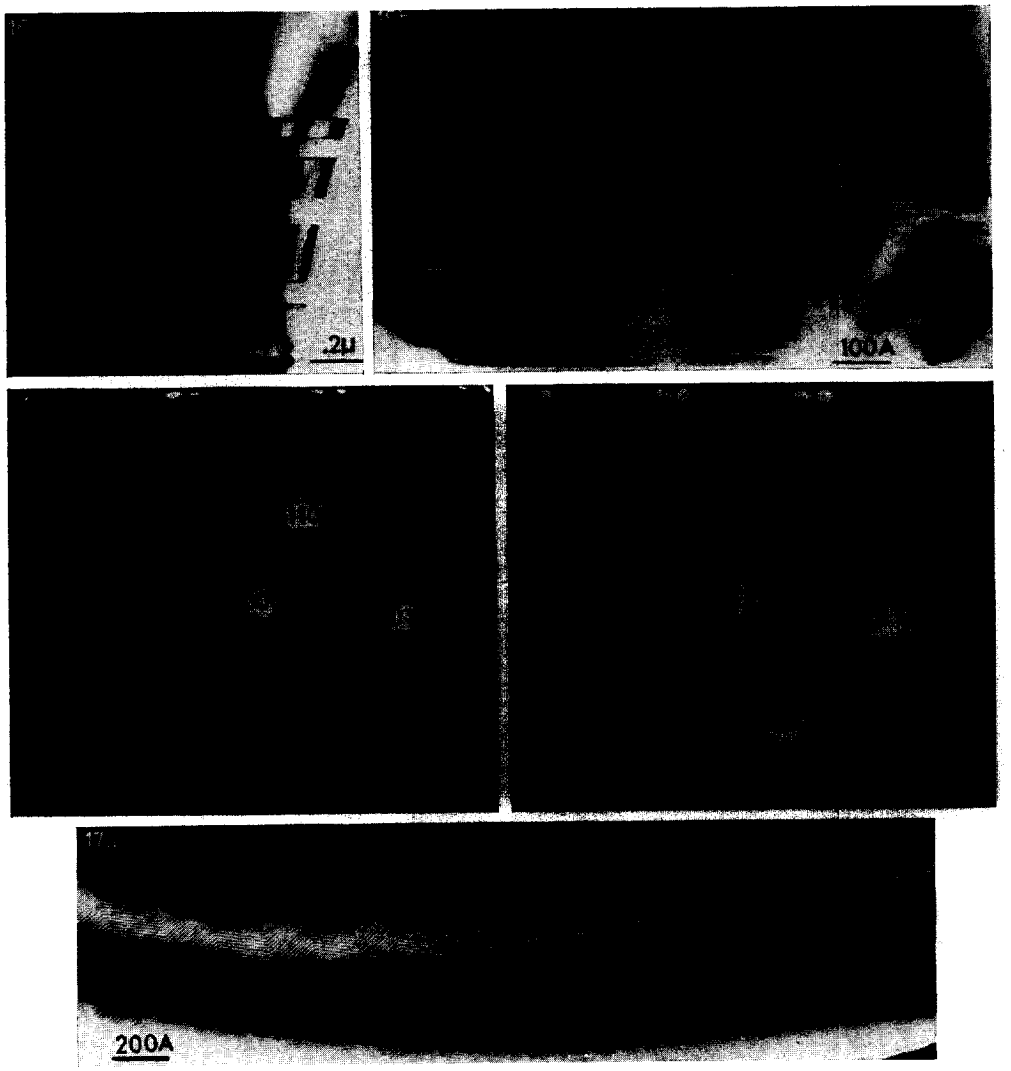

FIG. 16. (a) $(Ti,Fe)O_{1.975}$(1.8). Rutile microtwins with (011) composition planes.
(b) Irregular spacings and misorientations within a microtwin.
(c, d) [1$\bar{1}$1] zone showing two degrees of development of spots in rutile twin positions.

FIG. 17. (a) $(Ti,Fe)O_{1.95}$(2.2). Zig-zag lamellae of ordered {253} faults, spacings of approx 31 Å correspond to $MX_{1.96}$. Note the remarkable continuity across many twin boundaries, composition plane (100).

appeared (cf. 1.3). Many flakes of pseudobrookite occurred.

3.2 [1450°C, 7 days, sealed tube]. Ordered lamellae of {253} *CS* structures predominated with spacings corresponding to $MX_{1.935-1.946}$. Some poorly ordered wobbly *CS* planes (*1*) occurred. The *CS* plane was always between (132) and (121) and the mean stoichiometry was $MX_{1.94}$, the same as for the ordered structures.

3.3 [1500°C, 7 days, sealed tube]. Ordered lamellae of (495) *CS* structures occurred with $MX_{1.935-1.940}$. Pseudobrookite and the (100)-derived structure were also found.

3.4 [1500°C, 7 days, then 1200°C, 20 days, open tube]. Pseudobrookite occurred but

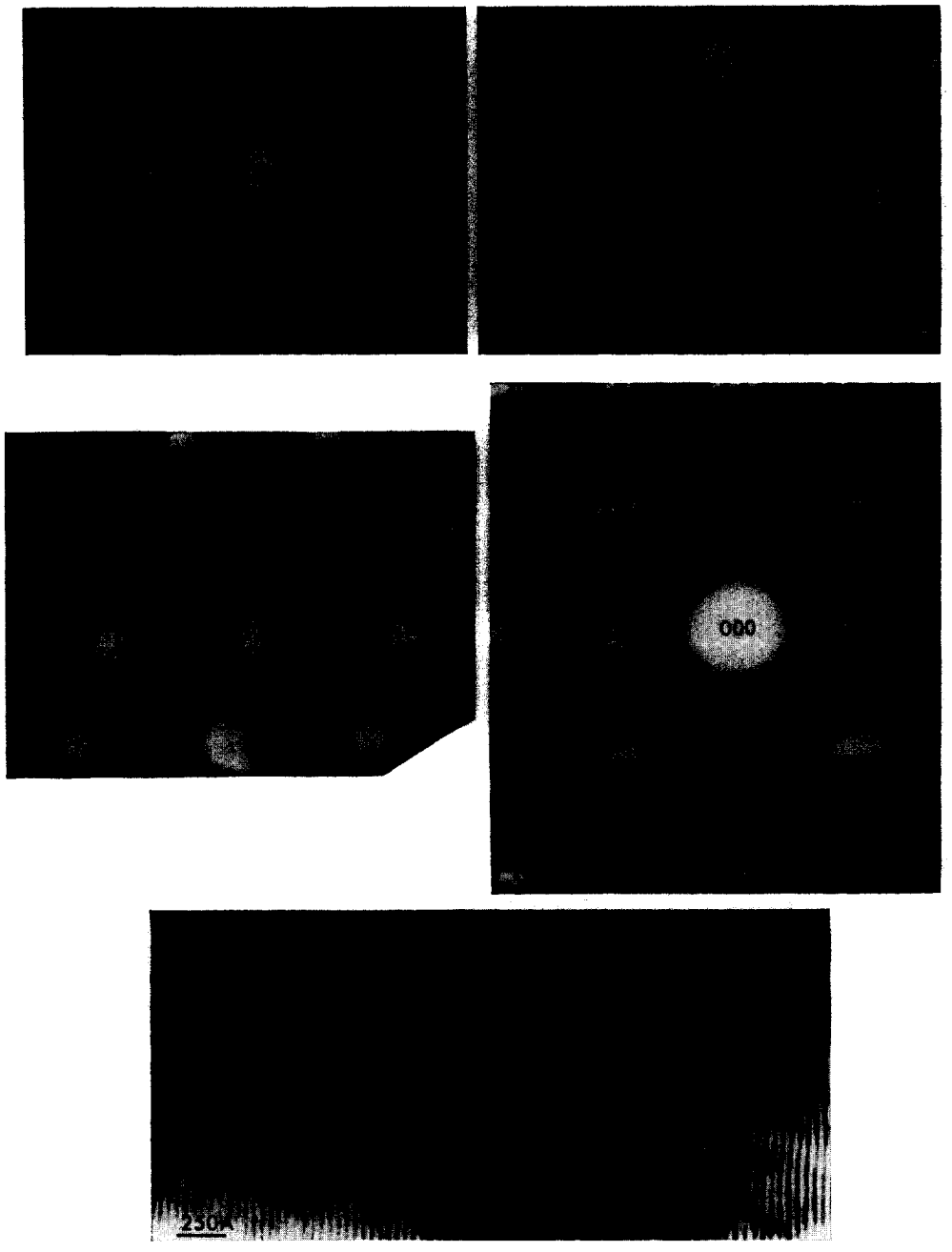

FIG. 17 (b) [1$\bar{1}$1] zone showing disordered high-index faults, both the orientation (approx (253)) and the spacing (approx 30 Å) vary.
(c) [1$\bar{1}$1[zone showing (121) structure with $n = 16$, i.e., $MX_{1.938}$.

FIG. 18. $(Ti,Fe)O_{1.95}(2.4)$. [1$\bar{1}$1] zone showing intense diffuse scattering around rutile positions.

FIG. 19 (a) $(Ti,Fe)O_{1.95}(2.4)$. Superstructure based on (100) structure with 28.5 Å period.
(b) High-resolution image of 19(a) using central beam and several spots on either side.

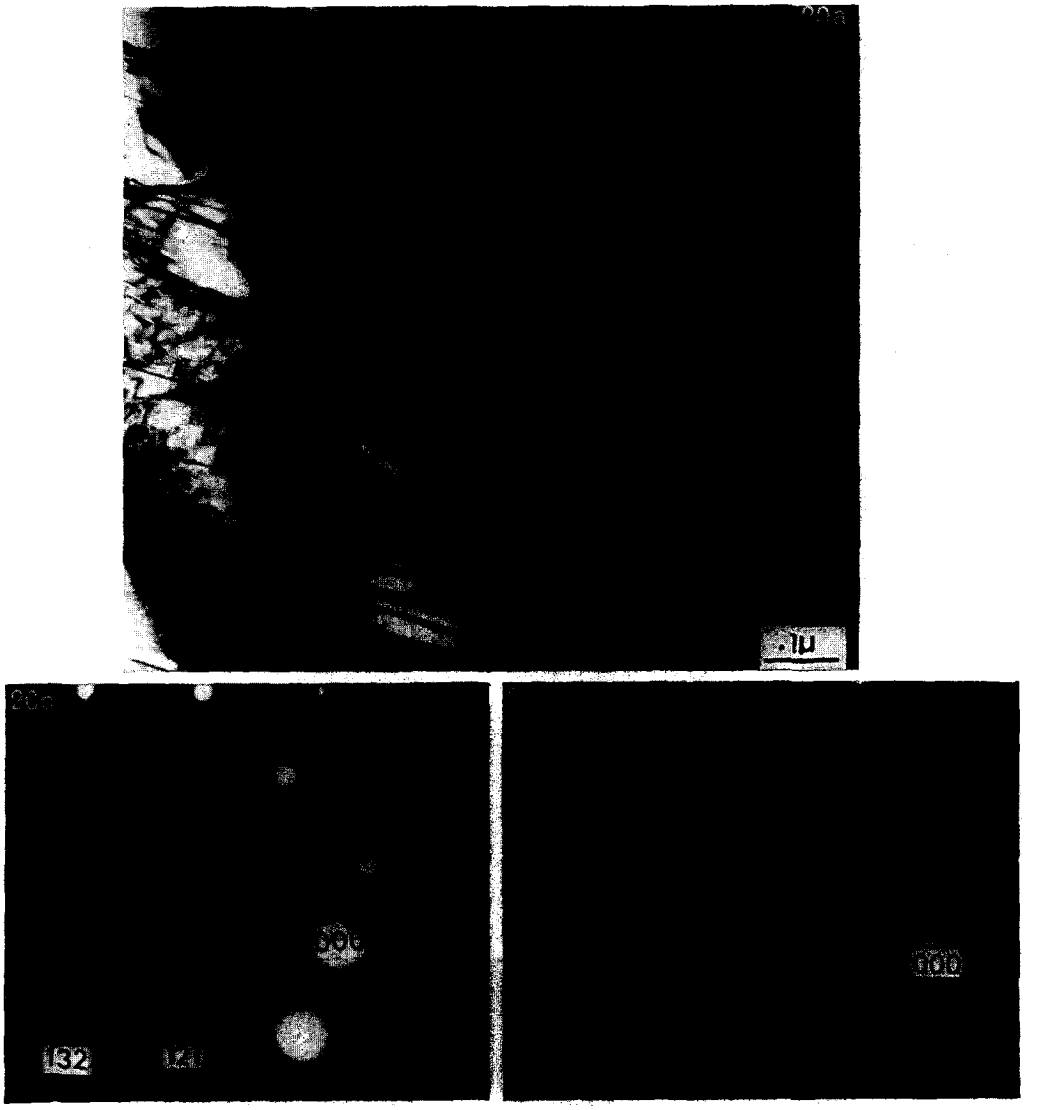

FIG. 20. (a) $(Ti,Fe)O_{1.95}$(2.6). Segregation into bands of zig-zag {121} faults plus bands of rutile containing a low density of {132} faults.
(b) [1$\bar{1}$1] zone of 20(a) showing streaking along both 121 and 132.
(c) [1$\bar{1}$1] zone showing streaking along 143.

predominant was a low density of {132} faults in rutile ($MX_{1.999}$). The dislocation density, which was negligible at 1300°C, was again very high.

4. (Ti, Fe)$O_{1.80}$

4.1 [1300°C, 14 days, sealed tube]. Pseudobrookite predominated (cf. Fig. 9). Complex wavy domain boundaries appeared in beam-heated specimens (Fig. 21a). High-resolution images (Fig. 21b) showed 9.8 Å $(100)_{pb}$ fringes displaced at domain boundaries, the magnitude depending on the curvature of the boundary (the phase angle $\alpha = 2\pi g.R$ varies along the boundary). The 4.6 Å $(001)_{pb}$ fringes cross undeviated ($\alpha = 0$ or $2\pi n$). Fig. 21*c* shows weak superlattice spots not previously reported.

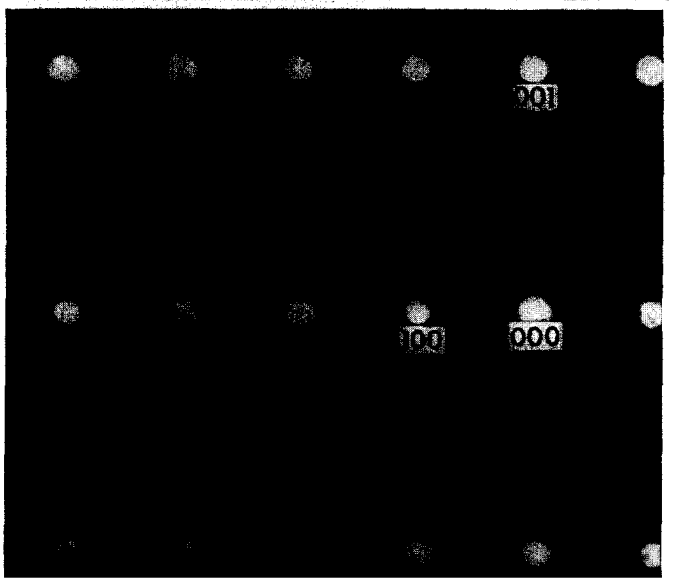
001
00
000

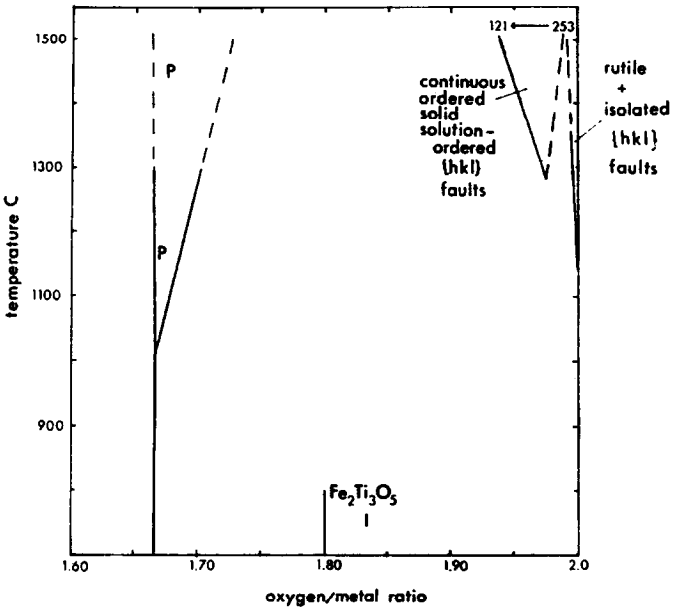

FIG. 22. Schematic revised phase diagram for FeO–Fe_2O_3–TiO_2 in air, constructed using all the observations summarized in Table I. Oxygen/metal ratio is plotted against temperature because the Fe^{3+}/Fe^{2+} ratios cannot be measured. Note the "continuous ordered solid solution" above 1300°C and the α-PbO_2-derived *CS* structure above 1450°C. The rutile field is very narrow ($MX_{1.995}$ at 1300°C).

Rutile containing a low density of {132} and {011} faults also occurred ($MX_{1.999}$). No {121} faults were found.

4.2 [1450°C, 7 days, sealed tube]. Pseudobrookite predominated.

4.3 [1500°C, 7 days, open tube]. As for 4.2.

4.4 [1500°C, 7 days, then 1100°C, 28 days open tube]. Pseudobrookite coexisted with rutile containing {011} and high-index faults close to {011} (cf. Fig. 15c).

Discussion

Phase analysis. The observations were combined to construct a schematic diagram, Fig. 22, which summarizes the observed structures. It refers only to samples heated in air and, since the Fe^{3+}/Fe^{2+} ratios can not be measured, we plot oxygen/metal ratio versus temperature. The following notes explain the derivation and interpretation of this diagram.

(*a*) *At 1300°C.* Although many crystals showed a subtle, ill-defined domain texture (Figs. 7c, 11a) which cannot be classified as one or two phase, it appears that, after sufficiently long anneals, they unmix into rutile containing isolated {132} *CS* planes plus lamellae of ordered {121} structure (1.1–1.3). This same texture was obtained independent of whether samples were annealed only at 1300°C or first equilibrated at 1500°C and then at 1300°C (see 1.3, 1.6, and 3.4) and therefore appears to be an equilibrium situation. Even isolated faults tend to align after long anneals (Fig. 10a). Annealing times at least one order of magnitude greater than used in previous studies were necessary.

FIG. 21. (a) $(Ti,Fe)O_{1.80}$(4.1). Wavy domain boundaries in beam-heated pseudobrookite.

(b) High-resolution image of 21(a). $(100)_{pb}$ fringes are displaced at the boundaries with magnitude depending on the orientation of the boundary. $(001)_{pb}$ 4.6 Å fringes are undeviated.

(c) $[010]_{pb}$ zone of 21(b) showing a new complex superstructure.

Introducing 0–0.5 mole% Fe_2O_3 into rutile produces widely dispersed {132} *CS* planes ($MX_{2.000-1.995}$). These tend to align but do not aggregate into lamellae, indicating very weak attractive forces. Further doping produces relatively closely spaced {121} *CS* planes aggregated into lamellae of stoichiometry $MX_{1.97}$ (3 mole% Fe_2O_3). Thus in the range 0.5–3.0 mole%, lamellae of $MX_{1.97}${121} coexist with $MX_{1.995}${132} with no intermediate high-index *CS* structures. The $MX_{1.97}${121} structure coexists with pseudobrookite for 3.0–33.3 mole% Fe_2O_3(2.1, 3.1, 4.1).

(*b*) *Below 1300°C.* At 1200°C, pseudobrookite coexisted with widely spaced {132} faults (approx $MX_{1.999}$) (see 1.6, 2.7, 3.4, 4.1), although a low density of {121} faults still occurred. At 1100°C, pseudobrookite coexisted with isolated faults whose indices were very close to {011} (see 1.7, 2.8, 4.4). No {121} lamellae were found. The {011} faults were accompanied by high concentrations of dislocations, singly, in tangles, or as walls (low angle grain boundaries) (see 1.7). As this defect structure was produced by first equilibrating at 1500°C and then annealing at 1100°C for 1 month, we must conclude that it is characteristic of the temperature and is not simply an incomplete reaction. Thus, at 1100°C, the rutile field is very small (less that $MX_{2.000-1.999}$) and iron appears to be accommodated at dislocations, grain boundaries, etc., as well as in pseudobrookite, i.e., the concentration of classical point defects must be extremely small.

(*c*) *Above 1300°C.* Ordered *CS* structures now appear giving rise to the region labeled "continuous ordered solid solution" in Fig. 22. This is apparently indistinguishable from "rutile" in X-ray and thermodynamic studies. Preparations in this composition–temperature range have *CS* planes whose indices and spacings vary continuously, not only with oxygen/metal ratio but also as a function of temperature. Thus at 1300°C, the *CS* plane is {121} with $n = 33$, i.e., $MX_{1.97}$ (coinciding with the rutile phase limit reported in Ref. (*5*)), whereas at 1450°C, the *CS* plane ranges from (253) to (121) with stoichiometry $MX_{1.97-1.935}$.

Thus increased temperatures enable elements of (121) and (132) *CS* structure, which completely unmix at 1300°C, to intergrow at unit-cell level, thus forming intermediate *CS* planes with $(hkl) = p.(121) + q.(011)$ (see Ref. (*1*)). At the same time, the lower limit of {121} structures decreases to smaller oxygen/metal ratios. Thus, at a given temperature, there is a range of compositions for which the *CS* plane swings continuously from approx (253) to (121), the width of this range increasing with increasing temperature. Since the n values (16–33 for (121)) are much larger than for Ti_nO_{2n-1}(4–9), the supercell spots are much closer and much weaker and all that is resolvable on X-ray powder photographs are the rutile subcell reflections. Thus for X-rays, this region appears to be a "solid solution". In a very real sense it is a solid solution, but at every point a different, perfectly ordered *CS* structure is found.

At temperatures above 1450°C and for mixtures containing 6–18 mole% Fe_2O_3, the {121} structures coexist with the (100)-derived *CS* structure (2,4, 3.3).

Pseudobrookite formed perfect crystal grains at all temperatures investigated (1200–1500°C). It was incoherent with rutile and mostly formed separate grains. It may occur as precipitates inside rutile flakes only for low doping concentrations (Fig. 8). The wavy domain boundaries and superstructure found in beam-heated pseudobrookite (Fig. 21) are of unknown origin. They may be related to the homogeneity range reported in Refs. (*2*, *5*) but could also indicate decomposition of ferric to ferrous pseudobrookite. An electron microscope study of pseudobookite would be interesting.

Reaction mechanisms. The mechanism of production, aggregation, ordering, and cooperative reorientation of *CS* planes in binary metal oxides was reviewed in Ref. (*1*). Although planar faults have been observed to extend in rutile by the splitting of dislocations into partials, there is no unambiguous evidence that *CS* planes nucleate inside the crystal or that either anion vacancy disc or interstitial cation disc dislocation mechanisms are involved. There are two fundamentally different ways of extending a *CS* plane into a crystal from the surface (Fig. 32, Ref. (*1*)),

one involves *no* point defects. The partial dislocation moves in the glide plane and there is a stoichiometry change only if the Burger's vector has a component normal to the surface (*1*). Formation of a *CS* structure by solid-state reaction in a ternary system, for example:

$$Fe_2Ti_{n-2}O_{2n-1} = Fe_2O_3 + (n-2)TiO_2$$

or

$$FeTi_{n-1}O_{2n-1} = FeO + (n-1)TiO_2,$$

requires long-range counter diffusion of both iron and Ti^{4+} ions. Since rutile is the major component, we consider diffusion of iron into rutile. Analogous reverse mechanisms will apply for Ti diffusing into, for example, Fe_2O_3. In general, both processes will take place in a reaction zone. We suppose initial sintering of Fe_2O_3 and TiO_2 produces deformation to relieve strain at randomly oriented, incoherent grain boundaries. Two slip systems may operate in rutile (*12*); perfect dislocations with Burger's vector [001] or extended dislocations (*APB*'s) $\{011\}\frac{1}{2}\langle 0\bar{1}1\rangle$. A perfect dislocation may dissociate into two *APB*'s:

$$[001] = (0\bar{1}1)\tfrac{1}{2}[011] + (011)\tfrac{1}{2}[0\bar{1}1].$$

Iron may add to the *APB* steps, eventually forming $[1\bar{1}1]$ chains at or near a surface (Fig. 4). The partial dislocation may then extend into a rutile grain, producing new steps on which new $[1\bar{1}1]$ chains form, and leaving a *CS* plane in its wake. Any *CS* plane $\{hkl\}\frac{1}{2}\langle 0\bar{1}1\rangle$ may be produced by the appropriate sequence of *A* and *C* type steps. The partial may stay just ahead of the growing *CS* plane or it may be separated from it by a segment of straight or irregularly stepped *APB*, depending on the local composition and the mechanical strain at the tip. Figures 15b, d, e and 7b show stepped and segmented {011} faults. Dotted strain contrast in 15b, d suggests that $[1\bar{1}1]$ chains are imperfectly formed, containing jogs or else not extending completely through the crystal. This non-equilibrium situation is expected for sample 1.7 which contained only Fe^{2+} and was annealed for only 1 day at the low temperature of 1100°C. Figure 7c shows another non-equilibrium crystal. Heating this sample for 14 days produced unmixing into $MX_{1.995}$(132) and $MX_{1.97}$(121). The high density of dislocations associated with {011} faults for 1.7, 1.8, and 4.4, again at relatively low temperatures, support the proposal that the initial reaction involves deformation of the rutile, either by perfect dislocations or *APB*'s. All of the observations, including the remarkable continuity of the *CS* planes in all situations, provide good evidence that the production, ordering, and cooperative reorientation of the *CS* planes is dependent on the formation and mobility of $[1\bar{1}1]$ chains of extra cations on the *APB*'s.

Our assumption that Fe^{3+} and Fe^{2+} are eventually located in face-shared pairs of octahedra will only be justified by accurate single-crystal structure analysis of ordered ternary structures. It does not appear to hold for Ti^{3+} in $(T_2^4i^+Ti_2^{3+})O_7$ (*13*). An alternative assumption, that Fe^{3+} (or Fe^{2+}) substitute for Ti_2^{4+} in normal octahedral sites, is equally consistent with all our observations. Oxygen "vacancies", one for every two Fe^{3+} and one for every Fe^{2+}, would then be eliminated at the partial dislocation producing identical $[1\bar{1}1]$ chains as for extra cations (see Fig. 21, Ref. (*1*)). Iron is then not necessarily tied to *CS* planes. Segregation into isolated {132} and aggregated {121} faults in samples 1.1–1.3 and the apparent increase of {121} faults at higher temperatures for 1.4 and 1.5 suggested that Fe^{3+} and Fe^{2+} were segregating to {132} and {121} faults, respectively. If so, this would confirm that the iron was located in the *CS* planes. Samples 1.7 and 1.8 were therefore prepared with Fe^{2+}. Surprisingly, neither {121}, or {132} faults were found, only closely spaced faults very close to {011}. Nevertheless, the *CS* plane indices are clearly dependent on the Fe^{3+}/Fe^{2+} ratio, indicating that the altervalent cations remain close to, if not on, the *CS* planes.

If partial dislocations *climb* into rutile crystals, extra cations (or anion vacancies) must diffuse to the fault tip and then add to it. Climb was observed in beam-heated rutile (*1*). Complicated diffusion paths are imposed whenever there is a significant density of *CS* planes. Thus sluggish reactions are expected, for example, unmixing of the crystallographic

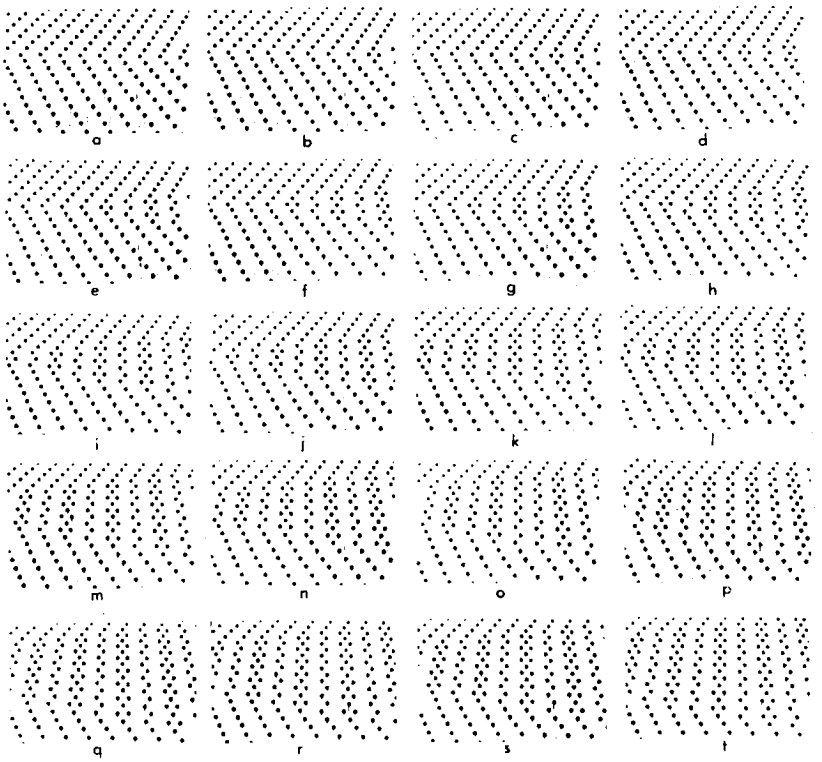

FIG. 23. (a, b) Introduction of a [1$\bar{1}$1] chain onto a microtwin boundary in rutile, producing an element of V_3O_5 structure.

(c) Diffusive hops move the [1$\bar{1}$1] chain along the twin composition plane leaving behind a lamellae of α–PbO_2 structure.

(d–t) Addition of further [1$\bar{1}$1] chains and the controlled movement of these into the crystal eventually produces a *CS* structure based on α–PbO_2; in this case it is $Fe_2Ti_3O_9$, but any of the many other possible intergrowth structures may be produced.

indigestion of Fig. 7a to give texture like Fig. 20a, and reaction at too low temperatures, will be choked-off. Such nonequilibrium preparations may explain hysteresis in thermodynamic studies of titanium oxides (*1*).

Fine-scale multiple twinning at high temperatures (1500°C) reflects the tendency for aggregated faults to zig-zag (Fig. 6d). Very diffuse diffraction patterns (Fig. 18) are characteristic of preparations quenched from near the melting point. Annealing out of twins was observed for some 1500°C anneals. Note that the melting point drops rapidly as the Fe_2O_3 content increases (Fig. 1a).

Transformation from rutile to α–PbO_2 structures. Preparations doped with Fe^{2+} contained microtwins (Figs. 15b, 16a–d) produced by repetition of the operation $(011)\frac{1}{2}[0\bar{1}1]$ on every (011) oxygen plane (Fig. 3d). Streaking along **g**(011) shows that the faults are not perfectly ordered. Stepping and misorientation of some faults occurs, indicating that the faults are nonstoichiometric. Samples with the same oxygen/metal ratio but containing only Fe^{3+} showed, at 1300°C, only {121} and {132} faults. Fig. 23a shows that a [1$\bar{1}$1] chain may be incorporated at a microtwin boundary, thereby introducing an element of V_3O_5. Diffusion of metals between adjacent PbO_2 zig-zag strips moves the [1$\bar{1}$1] chain along the twin composition plane (Figs. 23b, d), leaving behind a lamellae of α–PbO_2. Addition of further [1$\bar{1}$1] chains eventually produces α–PbO_2 *CS* struc-

tures (Fig. 23t). The structures observed in Figs. 15b and 16b may therefore be precursors to the $Fe_2Ti_5O_9$ found at low temperatures (Fig. 22). Further investigation of the FeO–TiO_2 system is necessary.

Acknowledgments

This work was supported by the Australian Research Grants Committee. The author wishes to thank Dr. B. G. Hyde for his interest in this work and Drs. A. F. Reid and I. E. Grey for sending preprints of their papers.

References

1. L. A. Bursill and B. G. Hyde, *Progr. Solid State Chem.* **7**, 177 (1972).
2. J. B. MacChesney and A. Muan, *Amer. Mineral.* **44**, 926 (1959).
3. A. H. Webster and N. F. H. Bright, *J. Amer. Ceram. Soc.* **44**, 110 (1961).
4. R. M. Gibb and J. S. Anderson, *J. Solid State Chem.* **5**, 212 (1972).
5. R. W. Taylor, *Amer. Mineral.* **49**, 1016 (1964).
6. A. F. Reid and J. C. Ward, *Acta Chem. Scand.* **25**, 1475 (1971)
7. I. E. Grey, A. F. Reid, and J. G. Allpress, *J. Solid State Chem.* (in press).
8. R. G. McQueen, J. C. Jamieson, and S. P. Marsh, *Science* **155**, 1401 (1967).
9. L. A. Bursill, B. G. Hyde, and D. K. Philp *Phil. Mag.* **23**, 1501 (1971).
10. L. A. Bursill and B. G. Hyde, *Proc. Roy. Soc. (London)* **A320**, 147 (1970).
11. L. A. Bursill and B. G. Hyde, *Acta Cryst.* **B27** 210 (1971).
12. K. H. G. Ashbee and R. E. Smallman, *Proc., Roy. Soc. (London)* **A274**, 195 (1963).
13. M. Marezio, D. B. McWhan, P. D. Dernier, and J. P. Remeika, *J. Solid State Chem.* **6**, 213 (1973).